ISSN 1392-1320 MATERIALS SCIENCE (MEDŽIAGOTYRA). Vol. XX, No. X. 2027

Acoustic Control Mechanism of Multilayer Composite Structure Based on Statistical Energy Analysis and Transfer Matrix Algorithm

Li Cheng CHENG, Su Jin TAO *

College of Automotive and Electrical Engineering, Harbin Cambridge University, 239 Haping Road, Xiangfang District, Harbin 150000, Heilongjiang Province, China

http://doi.org/10.5755/j02.ms.44773

Received 13 April 2026; accepted 27 May 2026

To overcome the limitations of traditional single-layer materials in broadband sound absorption and the inadequacy of existing simulation methods for complex composite structures, this study proposes a hybrid modeling framework that integrates Statistical Energy Analysis (SEA) and Transfer Matrix Method (TMM). A cross-scale theoretical model is established to map material micro-parameters (flow resistivity, porosity, tortuosity) to macroscopic SEA subsystem parameters, enabling precise low-frequency wave description via TMM and efficient mid-to-high frequency statistical energy characterization via SEA. Comparative simulations reveal a fundamental divergence between the two methods: at 16 Hz, pure TMM predicts a transmission loss (TL) of only 0.44 dB, whereas SEA predicts 48.62 dB – a discrepancy exceeding 48 dB – highlighting TMM's idealized infinite-layer assumptions versus SEA's system-level boundary considerations. Based on these findings, a frequency-domain weighted fusion model is developed, employing a Sigmoid weighting function calibrated by experimental data to achieve a smooth transition between the two methods across the full spectrum. The proposed SEA-TMM hybrid model reduces the root-mean-square error (RMSE) of TL prediction by 52 % compared to pure SEA and 93 % compared to pure TMM, providing a robust cross-scale theoretical tool for the high-performance design of complex multilayer acoustic materials.
Keywords: multilayer composite structure, acoustic tuning, statistical energy analysis, transfer matrix method, hybrid modeling.

1. INTRODUCTION

Noise pollution remains a critical challenge in modern industrial society, particularly in aerospace, rail transit, and architectural acoustics, where the demand for high-performance broadband sound-absorbing and sound-isolating materials is growing. Traditional single-layer porous materials often struggle to achieve both efficient sound absorption and isolation across wide frequency bands. Multilayer composite structures, especially those ingeniously combining porous layers with different characteristics, viscoelastic layers, and cavities, demonstrate significant potential for enhancing comprehensive acoustic performance through impedance matching and acoustic energy dissipation mechanisms. However, precise prediction of mid-to-high-frequency acoustic vibration responses poses challenges: pure statistical energy analysis (SEA) fails to accurately characterize interlayer coupling details, while pure transfer matrix method (TMM) proves inefficient in calculating high-frequency diffusion fields in complex structures. To address this, this study proposes and explores an innovative simulation framework based on a hybrid algorithm integrating statistical energy analysis and transfer matrix method (SEA-TMM), specifically designed for broadband acoustic characterization of multilayer composites. The core of this algorithm lies in: utilizing TMM to precisely describe intra-layer and interlayer near-field acoustic wave propagation and coupling mechanisms, while incorporating SEA to efficiently process high-frequency statistical energy flow and dissipation in subsystems. By establishing a theoretical bridge between material microstructural parameters (porosity, flow resistance, tortuosity, etc.) and macroscopic SEA subsystem parameters (modal density, coupling loss factor, internal loss factor) with TMM transfer matrices, this framework achieves efficient cross-scale modeling from material constitutive properties to system acoustic responses.

Juyue Ding [1] and colleagues investigated two types of automotive floor acoustic packaging: a conventional system composed of polyurethane foam and ethylene vinyl acetate (EVA), and a lightweight version made of polyurethane foam and polyethylene terephthalate (PET). Using Statistical Energy Analysis (SEA) to model both systems, they compared their sound transmission loss. The results demonstrated that while the lightweight packaging showed slightly lower sound transmission loss than the conventional one, it exhibited superior sound absorption performance and significant weight advantages. Rohit Ravindran [2] and his team conducted experiments with truck cabin materials including interior trim, carpets, and surface layers. By measuring parameters such as porosity, flow resistance, viscous characteristic length, and thermal characteristic length, they developed a SEA model to optimize acoustic packaging. This approach enabled them to achieve optimal noise reduction performance while maintaining quality control. Through testing 81 material combinations, they identified four optimal acoustic packaging solutions,

* Corresponding author: S.J. Tao
E-mail: *11947@hbuas.edu.cn*

validating the method as a time-and cost-efficient optimization strategy. Sachin Kumar Jain [3] and colleagues conducted research using melamine foam, placing samples of varying sizes into reverberation chambers of different dimensions to measure sound absorption coefficients. Based on the inherent parameters of melamine foam, they employed the Finite Transfer Matrix Method (FTMM) to predict its random incident sound absorption coefficients. The predicted results showed strong correlation with experimental measurements. The study demonstrated that large reverberation chambers could measure random incident sound absorption coefficients across the frequency range of 125 Hz to 10,000 Hz, and the FTMM predictions aligned well with chamber measurements. Aimin Du [4] and team investigated automotive front panel acoustic packaging, which consists of two layers: a sound-absorbing layer composed of 15 mm polyurethane (PU) foam and 10 mm felt, and an acoustic insulation layer made of ethylene-vinyl acetate with surface densities of 2 kg/m^2 and 4 kg/m^2, respectively. Through optimization of material parameters including thickness and coverage area, the team achieved noise reduction maximization at high frequencies while maintaining lightweight design. Pranab Saha [5] and colleagues investigated the typical structure of Dissipative Sound Package Systems (DSPS), emphasizing the importance of material composition in each layer. To meet lightweight requirements, DSPS compression layers must consider not only fiber selection and content control but also manufacturing parameters including temperature, processing time, and press tonnage. Jian Pan [6] and his team developed lightweight acoustic packaging materials to mitigate airborne noise. Their approach included: 1) a dual-layer acoustic panel combining lightweight structural fibers and polyurethane foam for superior thermal insulation and mechanical strength; 2) an ultra-lightweight PET acoustic panel with exceptional mechanical and sound-absorbing properties. In their mid-frequency noise analysis using hybrid Finite Element-Sound Absorption (FE-SEA) methodology, Kalpesh Mistry [7] developed a SEA model under road noise excitation and powertrain excitation, elaborated in detail on the challenges encountered during the modeling process, and also conducted research on the sensitivity of acoustic packages; these contributions provide valuable insights for constructing overall vehicle SEA models. These parameters were then incorporated into the FE-SEA model, enabling a comprehensive evaluation of interior noise control effectiveness. Shuming Chen [8] and colleagues employed grey relational analysis to determine the optimal combination of acoustic packaging parameters, utilizing principal component analysis (PCA) to calculate weight values related to multiple performance metrics. They optimized parameters of acoustic packaging materials in passenger vehicle interiors, including the thickness of soundproof panels on the outer side of firewalls, the thickness of sound-absorbing cotton on the inner side of firewalls, and the thickness of polyurethane foam at front and rear floor levels. Jesus et al. [9] proposed a calculation method based on the Voronina model to inversely determine the porosity, fiber diameter, and density of sound-absorbing materials, and the effectiveness of this inverse method was validated by experimental measurement results. Suvaria et al. [10] employed knitted materials made from polyethylene (PE) and polypropylene (PP) fibers with profiled cross-sections for compressed air devices, achieving favorable noise reduction performance. Under equivalent mass conditions, the knitted fibrous materials fabricated from trilobal PE fibers and 4DG-type PP fibers exhibited superior sound absorption performance compared to those made from fibers with circular cross-sections. Sound insulation materials play a crucial role in automotive noise reduction, which has prompted extensive research in this field. Sides [11] found in the theory of sound wave propagation in porous materials that, for porous materials, the orientation of fiber arrangement and fiber thickness are the primary factors influencing sound wave propagation.

The airflow resistance of porous materials can indirectly reflect the acoustic properties of the material itself. Biot [12] proposed the theory of elastic wave propagation in fluid-saturated porous media with an elastic framework. Subsequently, Attenborough [13, 14] built upon this foundation to develop a theory of acoustic wave propagation that is applicable not only to rigid porous materials but also to elastic porous materials. Multiple models and measurement techniques have since been investigated. Within this theoretical framework, the viscous and thermal conduction effects during sound wave propagation through porous materials, as well as fiber elasticity, fiber diameter distribution, shot content, and fiber orientation, are all taken into account.

Fouladi et al. [15] investigated the influence of an air cavity on the sound absorption performance of fibrous materials. The results indicated that as the cavity thickness increases, the first resonance frequency shifts toward lower frequencies, and the low-frequency sound absorption performance is significantly improved.

Xu Xiaomei [16] and colleagues investigated the acoustic properties of magnetorheological fluid sandwich panels, developing an acoustic finite element model. Their findings revealed that the low-order natural frequencies are primarily determined by structural stiffness, showing minimal variation with the excitation magnetic field. In contrast, high-order natural frequencies increase with rising magnetic field intensity. The study demonstrates that magnetorheological fluid sandwich panels exhibit superior sound insulation performance compared to other sandwich configurations.

2. MECHANISM OF SOUND ABSORPTION AND SOUND INSULATION OF POROUS MATERIALS

2.1. Sound absorption mechanism

When sound waves strike porous materials, they induce vibrations in the air and interstitial spaces within the pores and crevices. Due to frictional and viscous resistance between the material and air, as well as the material's thermal conductivity, a portion of the acoustic energy is converted into heat and dissipated. This energy dissipation is typically quantified by the sound absorption coefficient (α), a key metric for evaluating noise reduction performance of acoustic materials. The coefficient is defined as the ratio of the absorbed acoustic energy to the incident acoustic energy, expressed as follows:

$$\alpha = \frac{E_\alpha}{E} = \frac{E - E_t - E_r}{E}, \tag{1}$$

where E is the total incident sound energy; E_α is the sound energy absorbed by the material; E_t is the transmission of sound energy; E_r is the reflective acoustic energy.

A diagram showing the wave propagation distribution when sound waves hit, as shown in Fig. 1.

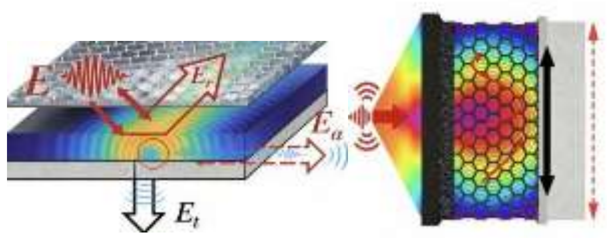

Fig. 1. Schematic diagram of wave propagation distribution during acoustic wave incidence

2.2. Sound insulation mechanism

When sound waves strike a material, some are absorbed, some are reflected back, and others propagate through the material. The sound insulation performance of a structure or material is typically measured by the sound insulation value, defined as the difference between the incident sound energy level and the transmitted sound energy level on the opposite side. This value is expressed by the equation:

$$TL = lg\left(\frac{E}{E_t}\right), \tag{2}$$

where TL stands for sound insulation, measured in dB.

When sound waves propagate through solid media, they typically exhibit three distinct zones: the stiffness-damping control zone, the mass control zone, and the resonance zone. In the low-frequency range (100 Hz – 6300 Hz), sound insulation performance is primarily governed by stiffness, which decreases with increasing frequency. As frequencies rise further, mass effects become dominant. At specific frequencies, the cancellation of stiffness and mass effects triggers resonance, where damping characteristics play a crucial role – this zone is termed the stiffness-damping control zone. In the mid-frequency range (630 Hz – 1250 Hz) and high-frequency range (> 1250 Hz), sound insulation improves with both mass and frequency, making mass effects the primary factor – this is known as the mass control zone. Solid media inherently possess elasticity. When sound waves at specific frequencies strike the medium at an angle and resonate with the bending vibrations induced by the incident waves, both the bending vibrations and sound radiation to the opposite surface reach their maximum amplitudes. This phenomenon, called the "resonance effect," occurs at a specific frequency known as the "resonance frequency".

3. TRANSFER MATRIX MODEL OF MULTILAYER COMPOSITE STRUCTURE

Transfer Matrix Method (TMM) is an efficient mathematical tool for analyzing wave propagation in layered media. The core principle of TMM is to decompose a multi-layered medium system into several homogeneous layers, transfer wave boundary conditions layer by layer through matrix operations, and ultimately solve the overall system response via the total matrix.

3.1. Multilayer material analysis model

To obtain the acoustic characteristic parameters of the multi-layer composite, a transfer matrix-based partial analysis model of the composite structure is established, as shown in Fig. 2.

Fig. 2. Theoretical model of the transfer distribution of a composite structure

The multi-layer composite is modeled as a combination of discrete thin layers for acoustic propagation analysis. A plane wave with wave number k is incident on the composite at an angle θ to the x-axis. The propagation relationship of the incident sound wave after passing through each thin layer is given as follows [17]:

$$V_1 = [T_{1n}]V_n, \tag{3}$$

where V_1 and V_n are the acoustic state vectors at the front and back surfaces of the composite material, respectively. The parameters for characterizing the state vectors of different media vary. The current total transfer matrix of the multilayer composite depends on the material properties of each layer and is coupled by the sub-transfer matrices of each discrete thin layer.

3.2. Analysis of acoustic transfer matrix of discrete interlayer materials

In multilayer composite acoustic materials, the discrete layers can be classified into four categories: fluid layer, solid layer, porous material layer, and viscoelastic layer. The state vectors between each medium are represented as follows [18]:

$$V^f(M) = \left[P(M), v_x^f(M)\right]^T; \tag{4}$$

$$V^x(M) = [v_x^x(M), v_y^x(M), \sigma_{xx}^x(M), \sigma_{xy}^x(M)]^T; \tag{5}$$

$$V^p(M) = \left[v_x^f(M), v_x^s(M), v_y^s(M), \sigma_{xx}^f(M), \sigma_{xx}^s(M), \sigma_{xy}^s(M)\right]^T, \tag{6}$$

where superscripts s, f, and p denote the fluid layer, solid layer, and porous material layer, respectively; $P(M)$ is the sound pressure value; V_x and V_y are the velocities of particles along the X-axis and Y-axis, respectively; σ_{xx} and σ_{xy} are the normal and tangential stresses of particles, respectively.

The transmission matrix of sound wave propagating in fluid medium is:

$$\begin{bmatrix} p(M_1) \\ v(M_1) \end{bmatrix} = \begin{bmatrix} cos(\, kd\, cos\, \theta) & j\frac{\rho c\, sin(kd\, cos\, \theta)}{\rho c} \\ j\frac{sin(kd\, cos\, \theta)}{\rho c} cos\, \theta & cos(\, kd\, cos\, \theta) \end{bmatrix} \times$$

$$\begin{bmatrix} p(M_2) \\ v(M_2) \end{bmatrix}, \tag{7}$$

where ρ is the flow field density; c is the sound velocity in the current environment.

When the sound wave enters the solid medium, it produces refracted longitudinal and transverse waves as well as reflected longitudinal and transverse waves. The corresponding displacement potential functions can be expressed as:

$$\varphi = C_1 e^{j(\omega t - k_y y - k_{yx} x)} + C_2 e^{j(\omega t - k_y y + k_{yx} x)}; \tag{8}$$

$$\psi = C_3 e^{j(\omega t - k_y y - k_{xx} x)} + C_4 e^{j(\omega t - k_{yy} + k_{xx} x)}, \tag{9}$$

where C_1, C_2, C_3, and C_4 are the amplitudes of the incident and reflected longitudinal and transverse waves, respectively; k_y is the Y-direction component of the sound wave; k_{xx} and k_{yx} are the wave numbers of the longitudinal and transverse waves in the X-direction.

Based on the fundamental elastic properties of solids, we hypothesize:

$$C^s = [(C_1 + C_2), (C_1 - C_2), (C_3 + C_4), (C_3 - C_4)]^T. \tag{10}$$

The state variable $V^s(M)$ of the solid layer can be expressed as:

$$V^s(M_n) = \Gamma(M_{n-1}) C^s. \tag{11}$$

The formula includes:

$$\Gamma(x) = \begin{cases} \omega k_y \cos(\, k_{yx} x) & -j\omega k_y \sin(\, k_{yx} x) \\ -j\omega k_{yx} \sin(\, k_{yx} x) & \omega k_y \cos(\, k_{yx} x) \\ -D_1 \cos(\, k_{yx} x) & jD_1 \sin(\, k_{yx} x) \\ jD_2 k_{yx} \sin(\, k_{yx} x) & -D_2 k_{yx} \cos(\, k_{yx} x) \end{cases}$$

$$\left. \begin{matrix} j\omega k_{xx}\, sin(\, k_{xx} x) & -\omega k_{xx}\, cos(\, k_{xx} x) \\ \omega k_y\, cos(\, k_{xx} x) & -j\omega k_y\, sin(\, k_{xx} x) \\ jD_2 k_{xx}\, sin(\, k_{xx} x) & -D_2 k_{xx}\, cos(\, k_{xx} x) \\ D_1\, cos(\, k_{xx} x) & -jD_1\, sin(\, k_{xx}) \end{matrix} \right\} \tag{12}$$

and

$$D_1 = \lambda(k_y^2 + k_{yx}^2) + 2\mu k_{yx}^2; \tag{13}$$

$$D_2 = 2\mu k_y^2. \tag{14}$$

Substituting x with 0 and t in Eq. 12 respectively, we obtain the sound wave propagation matrix in the solid layer:

$$T^s = \Gamma(0)\Gamma^{-1}(t). \tag{15}$$

For porous material layers, which integrate the characteristics of fluid laminated solid layers, the displacement potential function is defined as follows based on Biot's acoustic propagation theory for porous media [19]:

$$\varphi_1^s = C_1 e^{j(\omega t - k_y y - k_{yx} x)} + C_2 e^{j(\omega t - k_y y + k_{yx} x)}; \tag{16}$$

$$\varphi_2^s = C_3 e^{j(\omega t - k_y y - k_{zx} x)} + C_4 e^{j(\omega t - k_y y + k_{zx} x)}; \tag{17}$$

$$\psi_2^s = C_5 e^{j(\omega t - k_y y - k_{xx} x)} + C_6 e^{j(\omega t - k_y y + k_{xx} x)}; \tag{18}$$

$$\varphi_i^f = \mu_i \varphi_i^s (i = 1,2); \tag{19}$$

$$\psi_1^f = \mu_3 \varphi_2^s, \tag{20}$$

where C_i (i = 1,2,3,4,5,6) are six amplitudes; μ_i (i = 1,2,3) are all related to the material parameters of the porous material.

Similarly, the stress-strain relationship of porous materials leads to

$$C^p = \begin{bmatrix} (C_1 + C_2), (C_1 - C_2), (C_3 + C_4) \\ (C_3 - C_4), (C_5 + C_6), (C_5 - C_6) \end{bmatrix}^T. \tag{21}$$

The state variable $V^p(M)$ of the porous material layer can be expressed as:

$$V^p(M_n) = \Gamma(M_{n-1}) C^p. \tag{22}$$

After simplification, the transmission matrix of sound wave in porous material layer with thickness t is obtained:

$$T^p = \Gamma(0)\Gamma^{-1}(t). \tag{23}$$

3.3. Transfer matrix coupling

According to the continuity condition between each discrete layer, the transfer matrix of each medium is assembled to obtain the transfer matrix of the multilayer composite:

$$[I_{f,1}] V_1^f + [J_{f,1}] V_{M2}^f = 0; \tag{24}$$

$$[I_{k,k+1}] V_{M_{2k}}^k + [J_{k,k+1}] V_{M_{2(k+1)}}^f = 0 (k = 1,2,\cdots,n-1) \quad . \tag{25}$$

Acquirability:

$$D_m V_0 = 0; \tag{26}$$

These include:

$$D_m = \begin{bmatrix} I_{f,1} & J_{f,1} T^1 & 0 & 0 & 0 \\ 0 & I_{1,2} & J_{1,2} T^2 & 0 & 0 \\ \cdots & \cdots & \cdots & \cdots & \cdots \\ 0 & 0 & I_{(n-2)(n-1)} & J_{(n-2)(n-1)} T^{n-1} & 0 \\ 0 & 0 & 0 & I_{(n-1)n} & J_{(n-1)(n)} T^n \end{bmatrix}. \tag{27}$$

The total transfer matrix D can be obtained by combining the boundary conditions of the incident and transmitted ends of the composite material or the impedance equations of the sound pressure and velocity.

According to the definition of surface impedance of the medium, the surface impedance of the two ends of the composite can be expressed as:

$$Z_0 = p(M_1)/v_0^f(M_1); \tag{28}$$

$$Z_s = \frac{D'}{D''}, \tag{29}$$

where D' is the algebraic subdeterminant of the total transfer matrix after removing the first column element, and D'' is the algebraic subdeterminant of the total transfer matrix after removing the second column element.

When the end of the multilayer material is a rigid backing, the reflection coefficient and sound absorption coefficient of the multilayer composite can be expressed as:

$$R = \frac{Z_S \cos\theta - Z_0}{Z_S \cos\theta + Z_0}; \quad (30)$$

$$\alpha = 1 - |R|^2. \quad (31)$$

When the end of the multilayer material is a semi-infinite fluid domain, the transmission coefficient T and the reflection coefficient R have the following relation:

$$\frac{p(A)}{1+R} = \frac{p(B)}{T}. \quad (32)$$

Substituting Eq. 32 into the total transfer matrix, the transfer loss can be similarly derived.

$$TL = -10lg(|T(\theta)^2|). \quad (33)$$

4. EXPERIMENTAL DESIGN AND METHODS

4.1. Composite material selection

For this study, several representative sound-absorbing materials were selected to form porous composite structures through surface lamination. The selected composite materials are listed in Table 1.

Table 1. Composite material parameters

Material parameter	Perforated plate	Porous elastic polyester foam	Porous lightweight glass wool	Glass fibre
Thickness, m	0.01	0.0254	0.005	0.0254
Porosity	0.95	0.96	0.99	0.94
Rate of curving	–	1.24	1	1.2
Viscosity characteristic length, m	–	0.000105	0.000192	0.000104
Density, kg/m³	–	1.213	1.123	1.213
Poisson ratio	–	0.4	0	0
Young's modulus, N·m⁻²	–	46500	440000	0

4.2. Experimental methods

This study employs the widely used standing wave tube method to measure and investigate the acoustic properties of materials. The principle involves generating plane sound waves in a sealed pipe, measuring parameters such as the standing wave nodes and nodes formed by material reflection, as well as sound pressure levels. These measurements are then used to calculate the material's sound absorption coefficient, transmission loss, and other acoustic performance metrics. The schematic diagram is shown in Fig. 3.

4.3. Calculation principle of experimental measurement of sound absorption coefficient and reflection coefficient

When sound waves propagate from right to left, the incident sound wave can be expressed as [22]:

$$p_i = p_0 \, exp(j(\omega t + k_i x)). \quad (34)$$

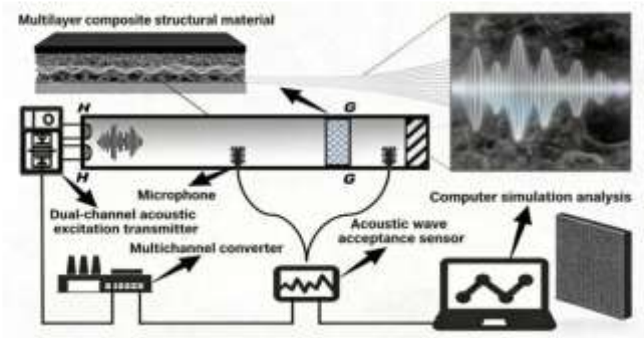

Fig. 3. Schematic diagram of the measurement using the travelling wave tube method [20]

The experimental apparatus and schematic diagram are provided in Fig. 4 and Fig. 5 respectively.

Fig. 4. Experimental apparatus [21]

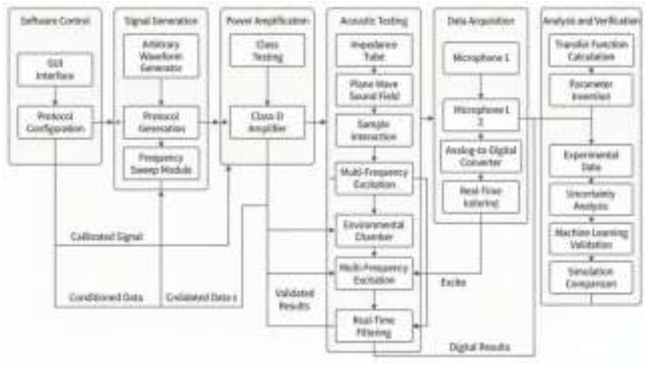

Fig. 5. Experimental principle block diagram

The reflected sound wave after total reflection of a plane incident sound wave through the cavity wall is:

$$p_r = p_0 \, exp(j(\omega t - k_r x)). \quad (35)$$

The plane incident sound wave and the reflected sound wave form a standing wave in the cavity after being combined, i.e.

$$p = p_i + p_r. \quad (36)$$

When no airflow passes through the cavity, the incident sound wave $k_i = k_r = k = \frac{\omega}{c}$ and the reflected sound wave have equal wave numbers. That is, when airflow passes through the cavity (assuming the airflow direction is from right to left, with velocity v and Mach number M), the incident sound wave's wave number is:

$$k_i = \frac{\omega}{c-v} = \frac{k}{1-M}. \quad (37)$$

The wave number of the reflected sound wave is:

$$k_r = \frac{\omega}{c+v} = \frac{k}{1+M} \quad (38)$$

Therefore, the standing wave within the cavity is:

$$p = p_i + p_r = p_0 \, exp(j\omega t)(exp(jk_i x) + exp(-jk_r x)) \, . \quad (39)$$

from the linearized momentum equation:

$$\rho \frac{\partial u}{\partial t} = -\frac{\partial p}{\partial x}. \quad (40)$$

Acquirability:

$$u = -\frac{p_0}{\rho c k} exp(j\omega t)(k_i \, exp(jk_i x) - k_r \, exp(-jk_r x). (41)$$

The velocity at point G-G is given by the condition of continuous velocity.

$$u_G = -\frac{p_0}{\rho c k} exp(j\omega t)(k_i \, exp(jk_i x_G) - k_r \, exp(-jk_r x_G)). \quad (42)$$

Substituting x_H=0 into Eq. 35, Eq. 36, and Eq. 37, we obtain:

$$p_H = 2p_0 \, exp(j\omega t). \quad (43)$$

Substituting into Eq. 42 yields:

$$u_G = -\frac{p_H}{2\rho c k}(k_i \, exp(j_k x_G) - k_r \, exp(-j_k x_G)). \quad (44)$$

According to the definition of sound impedance, we can get:

$$z_G = \frac{p_G}{u_G} = -\frac{p_G}{p_H} \rho c \frac{2k}{(k_i \, exp(j_k x_G) - k_r \, exp(-j_k x_G))}; \quad (45)$$

hypothesis:

$$\begin{cases} p_G = p_G' \, exp(j(\omega t + \phi_G)) \\ p_H = p_H' \, exp(j(\omega t + \phi_H)) \end{cases}. \quad (46)$$

Then the relative sound impedance rate at G-G is:

$$z = \frac{z_G}{\rho c} = -\frac{p_G}{p_H} exp(j(\phi_G - \phi_H)) \frac{2k}{(k_i \, exp(jk_i x_G) - k_r \, exp(-jk_r x_G)}. \quad (47)$$

The reflection coefficient of plane sound wave at G-G is:

$$R = \frac{z-1}{z+1}. \quad (48)$$

The sound absorption coefficient of the obtained composite is:

$$\alpha = 1 - |R|^2. \quad (49)$$

According to the Eq. 47, Eq. 48, and Eq. 49, the sound absorption coefficient and the sound reflection coefficient of the composite material can be obtained by measuring the sound pressure amplitude and the phase difference of the sound pressure at the point G and the point H.

4.4. Principles of sound pressure level calculation

In acoustics, sound intensity (I) is defined as the energy flux per unit area and time through a sound wave, and it is directly proportional to the square of sound pressure.

$$I = \frac{p_{rms}^2}{\rho c}, \quad (50)$$

where p_{rms} is the effective sound pressure; ρ is the medium density, and c is the speed of sound.

The sound pressure level is defined as the ratio of the actual sound intensity to the reference sound intensity, expressed as the logarithm of 10 and then multiplied by 10.

$$L_p = 10 \, log_{10}\left(\frac{I}{I_0}\right) \, (dB), \quad (51)$$

The reference sound intensity I_0 is typically defined as the sound intensity corresponding to the auditory threshold in air.

$$I_0 = \frac{p_0^2}{\rho c}, p_0 = 2 \times 10^{-5} \, Pa. \quad (52)$$

Substituting the relationship $I \propto p^2$:

$$\frac{I}{I_0} = \frac{p_{rms}^2/(\rho c)}{p_0^2/(\rho c)} = \left(\frac{p_{rms}}{p_0}\right)^2. \quad (53)$$

Substituting the logarithmic operation yields:

$$L_p = 10 \, log_{10}\left(\frac{p_{rms}}{p_0}\right)^2 = 20 \, log_{10}\left(\frac{p_{rms}}{p_0}\right). \quad (54)$$

5. SIMULATION OF MULTILAYER COMPOSITE STRUCTURE BASED ON TRANSFER MATRIX METHOD (TMM)

The TMM simulations in this section accurately capture the modulation of low-frequency sound absorption and reflection by microstructural parameters, revealing the broadband benefits of synergistic tortuosity and porosity design. In contrast to TMM applications by Rui et al. [23] for micro-perforated panels, which predict transmission loss primarily from macroscopic geometry, the present study extends TMM to multilayered porous composites by establishing a cross-scale mapping from pore-scale parameters (e.g., flow resistivity, characteristic lengths) to the state vectors of fluid, solid, and porous layers. This provides a more fundamental theoretical tool for the low-frequency design of complex acoustic materials.

5.1. Investigation of the influence of composite material curvature and porosity on sound absorption coefficient

For the porous elastic polyester foam, we adopted a 0.2 increment in both bending rate and porosity. For the composite of porous elastic polyester foam and glass fiber, we used the synergistic variables of bending rate and porosity, with interchangeable variables, to serve as controls and optimize single-variable results, investigating their effects on the sound absorption coefficient. The results are shown in Fig. 6, Fig. 7, Fig. 8, and Fig. 9.

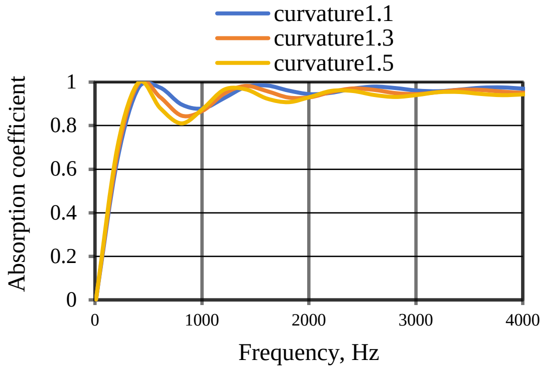

Fig. 6. Effect of different curvatures on the sound absorption coefficient of porous elastic polyester foam

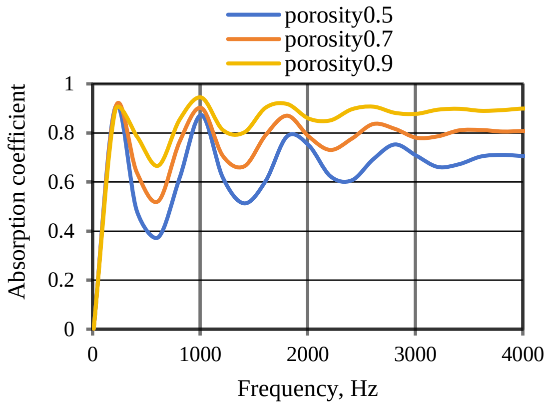

Fig. 7. Effect of different porosity on the sound absorption coefficient of porous elastic polyester foam

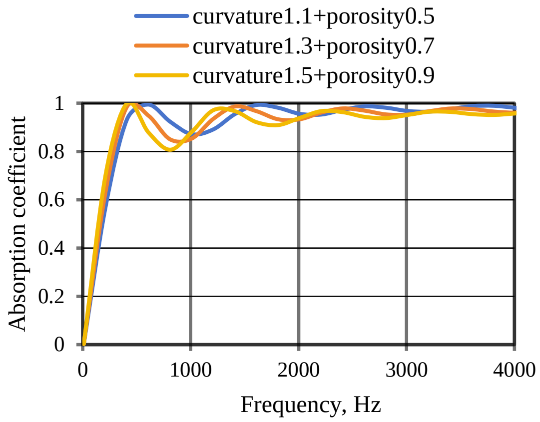

Fig. 8. Effect of synergistic variables of porosity of glass fibre and curvature of porous elastic polyester foam on sound absorption coefficient

Simulation studies using the Transfer Matrix Method (TMM) on composite material sound absorption coefficients demonstrate that microstructural parameters (e.g., flexural modulus and porosity) significantly modulate acoustic performance, with effects exhibiting strong frequency dependence. Fig. 6 and Fig. 7, respectively illustrate the impact of single-variable parameters (flexural modulus and porosity) on sound absorption coefficients in porous elastic polyester foam. At low frequencies (e.g., 10 Hz), all samples exhibit near-zero sound absorption coefficients, indicating limited acoustic wave penetration.

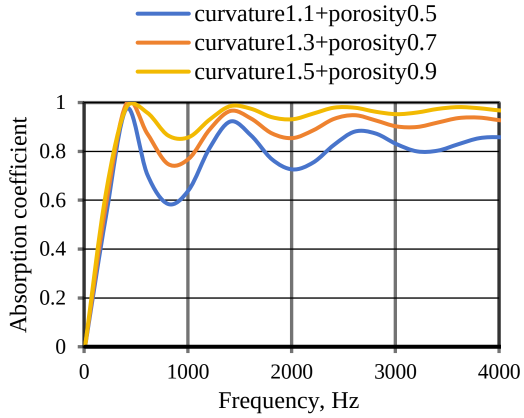

Fig. 9. Effect of porosity of porous elastic polyester foam and synergistic variable of glass fibre curvature on sound absorption coefficient

As frequency increases, absorption coefficients rise sharply between 210 – 410 Hz, peaking around 410 Hz (with maximum values approaching 1), reflecting intense resonant absorption within this frequency range. Subsequent fluctuations show a declining trend in mid-to-high frequency ranges (600 – 4800 Hz) while maintaining high levels (> 0.85), demonstrating the material's broad-frequency sound absorption potential. Comparative analysis reveals that increased flexural modulus enhances mid-low frequency absorption performance (Fig. 6), whereas higher porosity shifts the absorption peak toward lower frequencies and broadens the effective frequency band (Fig. 7).

Fig. 8 and Fig. 9 investigate the synergistic effects of porous elastic polyester foam and glass fiber on sound absorption performance. The results in Fig. 8 demonstrate that when the porosity of glass fiber and the flexural modulus of polyester foam are used as synergistic variables, the sound absorption curve achieves further optimization across a wide frequency range. Notably, the overall sound absorption coefficient in the 1200 – 3000 Hz band exceeds that of single-variable configurations, indicating that this parameter combination enhances interlayer impedance matching and promotes sound energy transmission and dissipation. Fig. 9 reveals that adjusting the synergistic interaction between polyester foam porosity and glass fiber flexural modulus can achieve lower reflection coefficients and higher sound absorption efficiency at high frequencies (> 3000 Hz), further validating that gradient design can optimize broadband sound absorption performance.

Low-frequency sound absorption is primarily governed by material intrinsic impedance and structural resonance, whereas mid-to-high frequency performance is closely associated with interlayer coupling, impedance gradient, and wave interference effects. The findings of this study not only provide a theoretical foundation for parametric design of multilayer composite sound-absorbing materials, but also highlight the high precision and applicability of TMM in material-level acoustic mechanism analysis. Particularly, it is well-suited for investigating and preliminarily optimizing material intrinsic characteristics in the low-frequency range.

5.2. Investigation of the influence of composite material curvature and porosity on the reflection coefficient

For the porous elastic polyester foam, we adopted a 0.2 increment in both bending rate and porosity. For the composite of porous elastic polyester foam and glass fiber, we used the synergistic variables of bending rate and porosity, with interchangeable variables, to serve as controls and optimize single-variable results, investigating their effects on the reflection coefficient. The results are shown in Fig. 10, Fig. 11, Fig. 12, and Fig. 13.

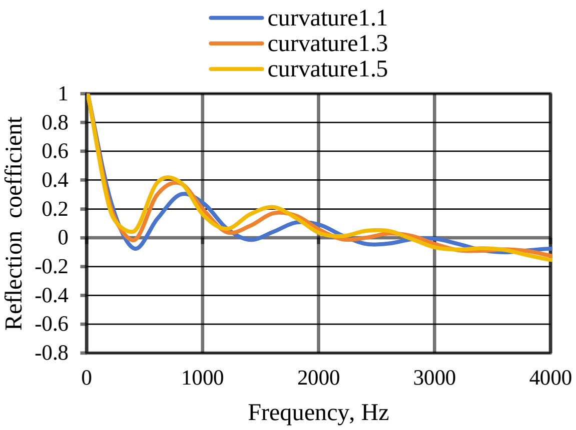

Fig. 10. Effect of different curvatures of porous elastic polyester foam on the reflection coefficient

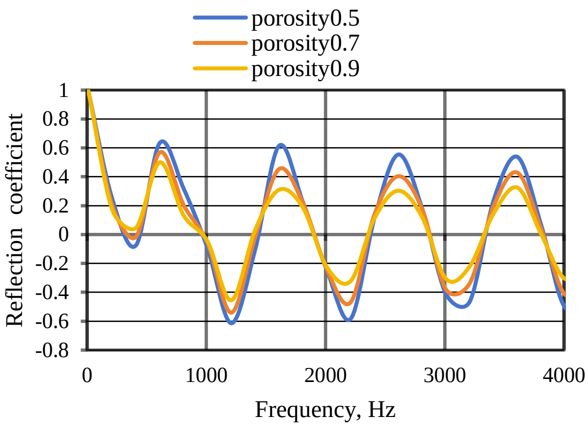

Fig. 11. Effect of different porosity of porous elastic polyester foam on the reflection coefficient

The simulation study of composite material reflection coefficients using the Transfer Matrix Method (TMM) further reveals the regulatory mechanism of material microstructure parameters on acoustic wave reflection behavior, demonstrating significant frequency dependence and parameter synergistic effects. Fig. 10 illustrates the impact of flexural curvature on reflection coefficients in porous elastic polyester foam. At low frequencies (< 500 Hz), all samples exhibited near-1 reflection coefficients, indicating that most acoustic energy was reflected. The first reflection trough appeared around 410 Hz, with the sample at 1.1 curvature showing a negative reflection coefficient (-0.0746), indicating significant phase cancellation interference and resonance absorption at this frequency.

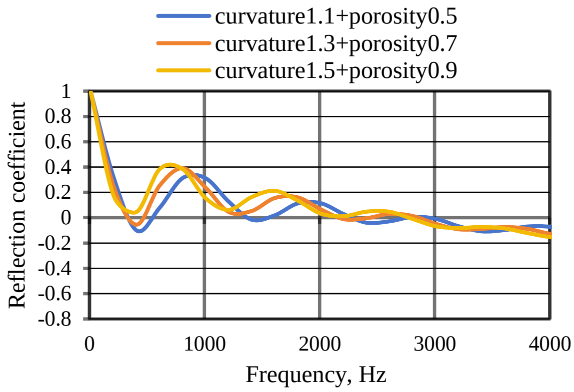

Fig. 12. Effect of synergistic variables of porous elastic polyester foam curvature and glass fibre porosity on the reflection coefficient

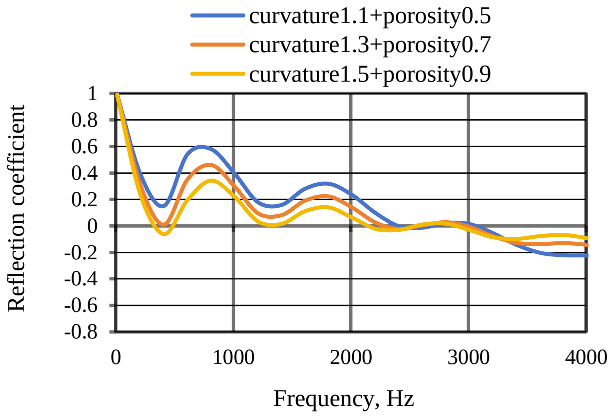

Fig. 13. Effect of porosity of porous elastic polyester foam and synergistic variable of glass fibre curvature on reflection coefficient

In the mid-frequency range (600 – 2000 Hz), reflection coefficients exhibited oscillatory characteristics, while all samples in the high-frequency range (> 3000 Hz) turned negative, further validating the material structure's phase modulation capability for high-frequency acoustic waves.

Fig. 11 investigates the single-variable effect of porosity on reflection coefficient in porous elastic polyester foam. The data demonstrates that porosity variations exert more complex modulation effects on reflection behavior, particularly in the mid-frequency range (e.g., at 1210 Hz, the reflection coefficient of a 0.5 porosity sample is-0.61395), exhibiting pronounced resonance absorption and impedance mismatch phenomena. These results indicate that increased porosity facilitates superior acoustic impedance matching in specific frequency bands, thereby reducing reflections and enhancing sound absorption.

Fig. 12 and Fig. 13 investigate the combined effects of bending curvature and porosity as synergistic variables on reflection characteristics. The results in Fig. 11 demonstrate that using polyester foam bending curvature and glass fiber porosity as synergistic variables yields superior control effects across a wide frequency range. Notably, the overall reflection coefficient in the 1200 – 3000 Hz band is lower than that of single-variable configurations, indicating that parameter synergy effectively optimizes interlayer impedance gradients and reduces overall reflection levels. Fig. 12 further reveals that adjusting the combination of polyester foam porosity and glass fiber bending curvature achieves lower reflection coefficients in the high-frequency range (> 3000 Hz), with the lowest value reaching -0.3411 at 4810 Hz. This demonstrates that the parameter synergy strategy exhibits enhanced phase inversion and energy capture capabilities for high-frequency acoustic waves.

6. SIMULATION OF MULTI-LAYER COMPOSITE STRUCTURE BASED ON ENERGY STATISTICAL METHOD

Statistical Energy Analysis (SEA) is a robust theoretical framework for predicting and analyzing the vibration and acoustic responses of complex dynamic systems under medium-to-high-frequency excitation. Unlike deterministic methods such as the Transfer Matrix Method (TMM), SEA is fundamentally a statistical approach based on energy flow.

The SEA analysis presented in this chapter predicts system-level transmission loss and elucidates the influence of thickness on mass-law and coincidence effects. Unlike prior SEA studies, such as Manning et al. [24] for reverberation chamber validation or Wang et al. [25] for vehicle wind noise combined with CFD, which treat panel properties as macroscopic inputs, our approach derives SEA subsystem parameters (modal density, internal loss factor, coupling loss factor) directly from material micro-parameters (porosity, tortuosity). This establishes a direct link between intrinsic material properties and statistical energy response, thereby enhancing the physical fidelity of mid-to-high frequency SEA predictions.

6.1. Statistical modeling of SEA energy in resonance chamber

The reverberation chamber method, a widely used technique for measuring material sound absorption and insulation coefficients, features rapid response capabilities. Essentially, this method creates an acoustic cavity where sound energy undergoes thorough reflection and diffusion, achieving uniform distribution. By precisely calculating the sound attenuation rate within this chamber, we can determine the material's acoustic absorption properties.

Using the simulation software VAONE, we established a reverberation chamber acoustic cavity and a multi-layer composite structure. The modal behavior of the materials was investigated by applying a 1 Pa diffuse sound field excitation, as shown in Fig. 14.

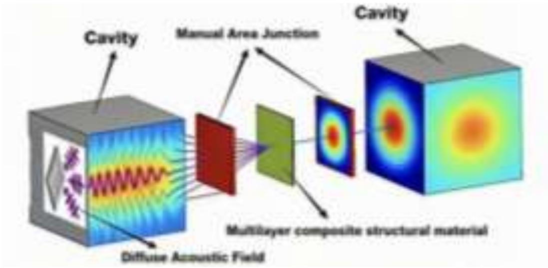

Fig. 14. Schematic diagram of reverberation chamber acoustic modelling

6.1. Global modal and sound pressure level cloud map of composite structure

The modal sound pressure level contour map (Fig. 15) of this multi-layer composite structure in the 0 – 200 Hz low-frequency range exhibits dispersed modal patterns and sparse distribution, indicating low modal density and strong local vibration response in this frequency band. These characteristics make it difficult to meet the core assumptions of Statistical Energy Analysis (SEA) for modal density and energy statistics.

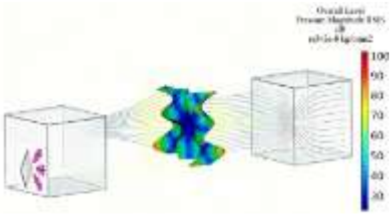

Fig. 15. A (0 – 200 Hz)

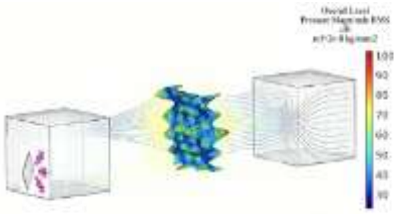

Fig. 16. B (200 – 400 Hz)

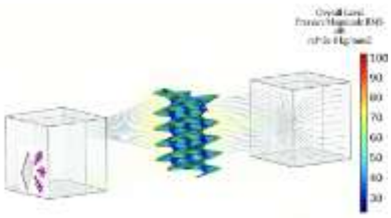

Fig. 17. C (400 – 600 Hz)

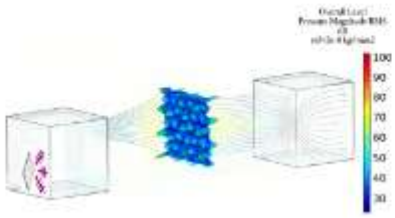

Fig. 18. D (600 – 1400 Hz)

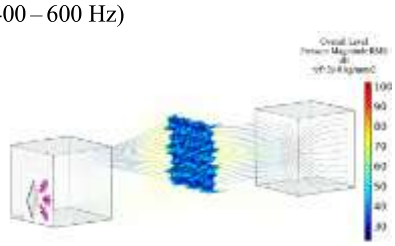

Fig. 19. E (1400 – 2500 Hz)

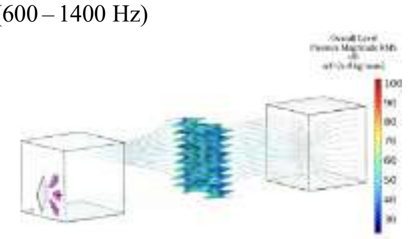

Fig. 20. F (2500 – 4000 Hz)

Consequently, SEA methods demonstrate limited accuracy in analyzing the structure's acoustic response at this low-frequency range, making deterministic approaches like the Transfer Matrix Method (TMM) more suitable. As the excitation frequency increases from 200 – 400 Hz to 400 – 600 Hz, the density and orderliness of the cloud patterns progressively enhance (Fig. 15, Fig. 16). When entering the mid-high frequency range above 600 Hz, the periodicity and global characteristics of modal shapes become significantly more pronounced (Fig. 17, Fig. 18). The finite element method excels at capturing the coupling mechanism between structural modes and acoustic fields in this frequency band, making it particularly suitable for analyzing low-frequency deterministic vibrations and acoustic radiation. This phenomenon demonstrates that the modal density of multi-layer composite structures increases with frequency, while vibration coupling between structural layers intensifies. Energy transfer behavior aligns more closely with the statistical assumptions of the Subsystem Energy Analysis (SEA) method based on subsystem energy flow, indicating that SEA's application conditions progressively meet within this frequency range.

The medium and high frequency acoustic noise reduction or vibration control can be optimized by SEA method like shown in Fig. 19, to improve the energy dissipation layer parameters of multi-layer structure, and the statistical energy transfer law of medium and high frequency can be used to improve the noise reduction efficiency.

6.3. Impact of composite structural material thickness on system transmission loss

To facilitate direct comparison between SEA and TMM algorithms, this study presents the sound insulation calculation using the SEA algorithm for composite structural materials, while exploring its fundamental control mechanisms.

The influence of the thickness increment of 5 mm on the transmission loss of the glass fiber and the thickness of the glass fiber and the honeycomb panel is investigated. Based on statistical energy analysis (SEA) of the impact of glass fiber thickness and its combined thickness with honeycomb panels on transmission loss (sound insulation), this study reveals the regulatory mechanism of thickness parameters on broadband sound insulation performance from a system energy statistics perspective. Fig. 20 demonstrates the influence of single glass fiber thickness (10 mm, 15 mm, 20 mm) on transmission loss. In the low-frequency band (16 – 100 Hz), sound insulation significantly improves with increasing thickness, exhibiting typical mass law characteristics. For instance, at 16 Hz, the sound insulation of a 20 mm thick structure (76.77 dB) is approximately 28 dB higher than that of a 10 mm thick structure (48.62 dB), indicating that increasing material surface density effectively enhances low-frequency sound insulation. In the mid-frequency band (125 – 500 Hz), a distinct sound insulation trough appears, related to the structural coincidence effect. As thickness increases, the trough position shifts slightly and its depth decreases, suggesting that thickness can partially suppress the degradation of sound insulation performance caused by the coincidence effect.

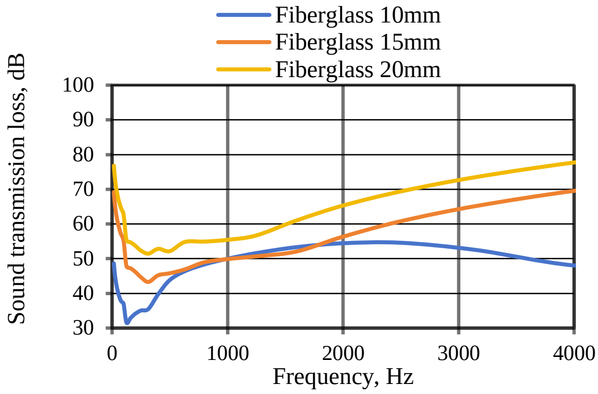

Fig. 21. The effect of composite structure glass fibre thickness on sound transmission loss

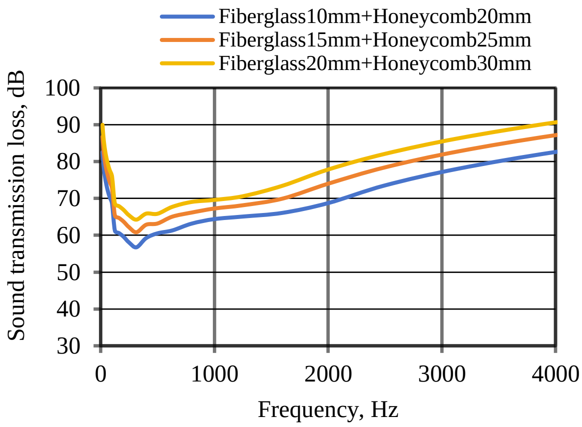

Fig. 22. Effect of the combined variable of composite structure glass fibre and honeycomb panel step thickness on sound transmission

In the high-frequency band (> 1000 Hz), sound insulation continues to rise with frequency, and the steeper the slope of the increase, the better the high-frequency sound insulation performance. For example, at 8000 Hz, the sound insulation of a 20 mm thick structure reaches 89.81 dB, approximately 32 dB higher than that of a 10 mm thick structure, demonstrating that high-frequency sound insulation is simultaneously influenced by mass effects and structural bending stiffness.

Fig. 22 further investigates the synergistic optimization effects of thickness gradient combinations between fiberglass and honeycomb panels on sound insulation performance. (Fiberglass 10 mm + Honeycomb 20 mm, Fiberglass 15 mm + Honeycomb 25 mm, Fiberglass 20 mm + Honeycomb 30 mm) all demonstrated superior sound insulation performance across the wide frequency range compared to single-layer thickening. In the low-frequency band, the Fiberglass 20 mm + Honeycomb 30 mm configuration achieved an impressive sound insulation level of 89.98 dB at 16 Hz, approximately 13 dB higher than the single 20 mm fiberglass layer. This indicates that multi-material layer thickening can more effectively enhance surface density and structural stiffness, thereby improving low-frequency sound insulation. In the mid-frequency range, the composite configuration exhibited shallower sound insulation valleys and faster recovery. For instance, at 400 Hz, the Fiberglass 20 mm + Honeycomb 30 mm configuration achieved a sound insulation level of 65.87 dB, significantly higher than the single 20 mm fiberglass layer (52.83 dB). This demonstrates that gradient thickness design optimizes interlayer impedance matching, effectively suppressing coincidence effects and promoting sound energy dissipation. In the high-frequency band, the composite configuration's sound insulation curve rises more rapidly. At 8000 Hz, the Fiberglass 20 mm + Honeycomb 30 mm configuration achieved a sound insulation level exceeding 102 dB, markedly surpassing the single-material thickening effect. This highlights the synergistic suppression of high-frequency sound wave transmission through material functional division and impedance gradient.

SEA simulations demonstrate that increasing material thickness significantly enhances the broadband sound insulation performance of composite structures. Specifically, the mass law governs low-frequency responses, while high-frequency performance is regulated by stiffness and impedance matching. The application of multi-material layer gradient thickness combinations further optimizes impedance matching, suppresses coincidence effects, and improves sound energy dissipation, achieving superior system-level sound insulation. These results validate the effectiveness and engineering applicability of SEA in evaluating mid-to-high-frequency system-level acoustic performance and multi-parameter collaborative optimization.

7. ACOUSTIC SYNTHESIS AND COMPARATIVE ANALYSIS OF MULTILAYER COMPOSITE STRUCTURE BASED ON TMM AND SEA ALGORITHMS

Having distinguished the two algorithms above, we now apply the same methodology to composite structures, focusing on comparative analysis of SEA and TMM's integrated results, including acoustic absorption coefficient, transmission loss, and damping loss factor.

The stark discrepancy between TMM and SEA predictions, exceeding 48 dB in low-frequency transmission loss and exhibiting opposite trends in damping loss factor, underscores that the two methods operate in distinct physical domains (ideal wave mechanics vs. real system statistics). While TMM models in Rui et al. [23] neglect finite-size effects due to idealized assumptions, SEA models in Manning et al. [24] and Wang et al. [25] suffer from modal sparsity at low frequencies. By directly quantifying these differences on an identical multilayer composite, this work delineates clear applicability boundaries: TMM is preferred for low-frequency material-level design, whereas SEA should govern mid-to-high frequency system-level evaluation. This data-driven guideline provides a robust foundation for hybrid modeling.

7.1. Comparative analysis of sound absorption coefficients

TMM (Twin-Matrix Method) is a deterministic approach based on wave theory, assuming the structure to be infinite, with homogeneous and isotropic materials across all layers. It calculates the sound absorption coefficient by precisely solving the reflection and transmission of plane waves at each layer interface. In the low-frequency range (e.g., 0 – 2500 Hz), TMM predicts an absorption coefficient close to 1 (Fig. 23, Fig. 24), indicating theoretically excellent sound absorption performance. However, TMM neglects the effects of finite dimensions, boundary conditions, and structural vibration modes in real-world structures, which may lead to overestimation of sound absorption performance in high-frequency applications or practical finite-size structures.

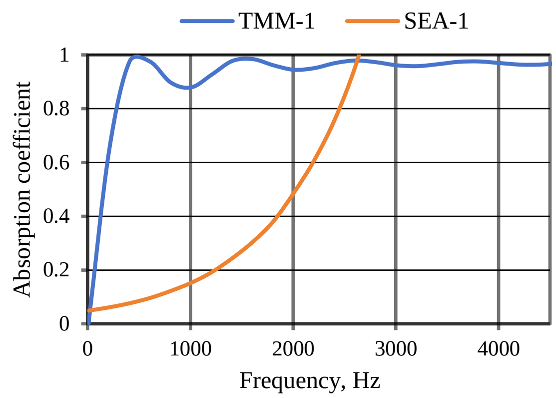

Fig. 23. Comparison of the effects of TMM and SEA algorithms on the sound absorption coefficient-1

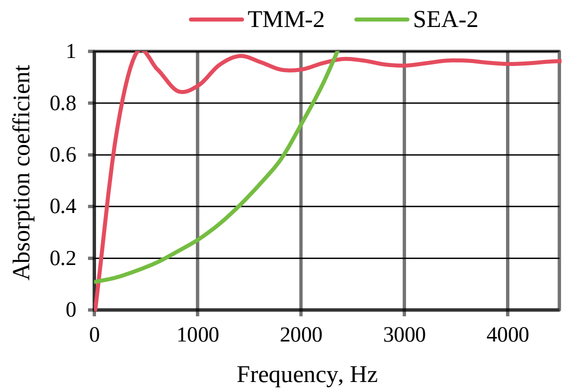

Fig. 24. Comparison of the effects of TMM and SEA algorithms on the sound absorption coefficient-2

SEA (Structural Energy Analysis) is an energy-statistical distribution-based method for vibration and acoustic analysis of complex medium-to-high frequency systems. It divides the structure into multiple subsystems and predicts acoustic responses by analyzing energy flow and dissipation. The SEA-derived sound absorption coefficient shows low values at low frequencies (e.g., 0.05) and gradually increases with frequency (exceeding 0.99). (Fig. 23, Fig. 24) This reflects SEA's consideration of modal density, coupling loss factors, and statistical excitation conditions, which more accurately captures the sound absorption behavior of finite-sized structures under actual diffused field excitation. At low frequencies, the sparse modal structure may render SEA's statistical assumptions (e.g., modal overlap, diffused field) invalid, leading to underestimated absorption coefficients. As frequency increases, the growing modal density satisfies these assumptions, causing the predicted absorption coefficients to approach the true values.

7.2. Comparative analysis of transmission losses

TMM predicts lower sound transmission loss (TL) at low frequencies (e.g., approximately 0.44 dB at 16 Hz), with a gradual increase to around 18 dB at 8000 Hz (Fig. 25 – Fig. 28), showing a generally gentle trend. While this reflects the mass law behavior of structures under ideal conditions, it neglects practical factors such as dimensional effects, boundary constraints, structural vibration coupling, and energy dissipation mechanisms. Consequently, it often underestimates sound insulation performance in real-world finite-size structures.

From a statistical energy perspective, SEA (Structural Energy Analysis) classifies structures into multiple coupled subsystems, describing energy flow and dissipation through modal density, coupling loss factor, and internal loss factor. SEA predicts significantly higher total sound energy (TL) overall (e.g., SEA-1 at 16 Hz reaches 48.6 dB, far exceeding TMM), with more complex fluctuation trends as frequency increases (Fig. 25 – Fig. 28).

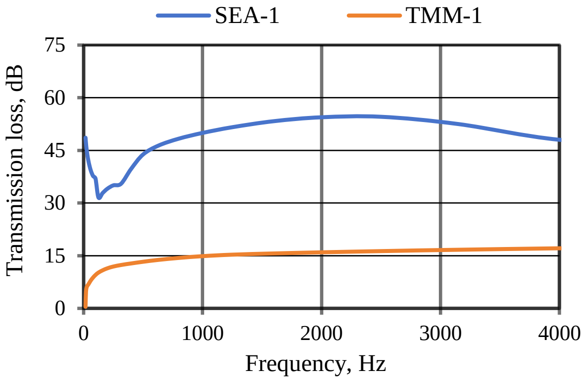

Fig. 25. Comparison of the impact of TMM and SEA algorithms on transmission loss-1

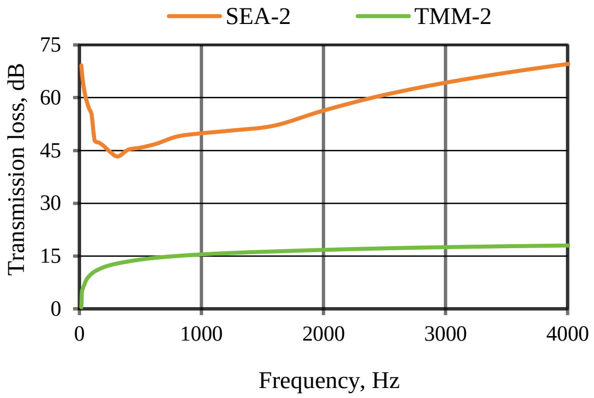

Fig. 26. Comparison of the impact of TMM and SEA algorithms on transmission loss-2

This is because SEA fully accounts for structural finite dimensions, modal responses, material damping, and energy transfer losses at interfaces, better reflecting the sound insulation behavior of composite structures in mid-to-high frequency ranges. Particularly in low-frequency bands, SEA's predicted sound insulation significantly exceeds TMM due to its consideration of boundary reflections and structural damping. At high frequencies, SEA yields more reliable results as modal density increases and energy distribution becomes statistically uniform.

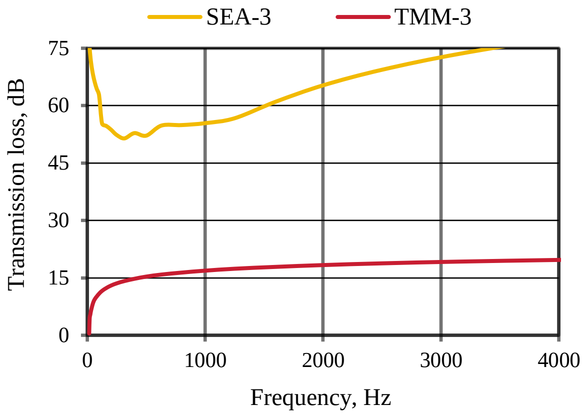

Fig. 27. Comparison of the impact of TMM and SEA algorithms on transmission loss-3

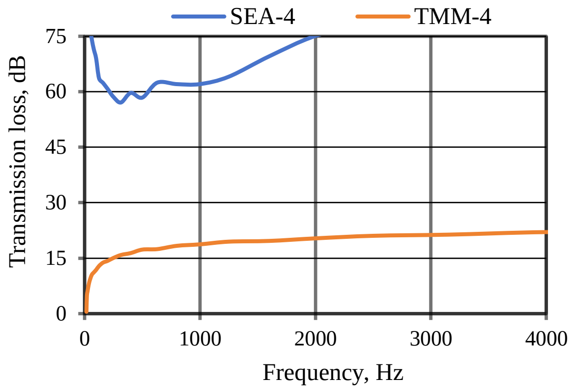

Fig. 28. Comparison of the impact of TMM and SEA algorithms on transmission loss-4

7.3. Comparative analysis of damping loss factors

The TMM (Twin-Mach-Mach) method derives damping based on the material's intrinsic complex modulus (complex stiffness or complex wavenumber). The calculated damping loss factor essentially represents the material's intrinsic internal friction (material loss factor). It assumes energy dissipation occurs exclusively within the material as volume dissipation in a homogeneous, continuous medium. Consequently, TMM predicted damping values are typically low (mostly below 0.12) and exhibit a gradual frequency-dependent variation, reflecting purely viscoelastic material properties (Fig. 29 – Fig. 32).

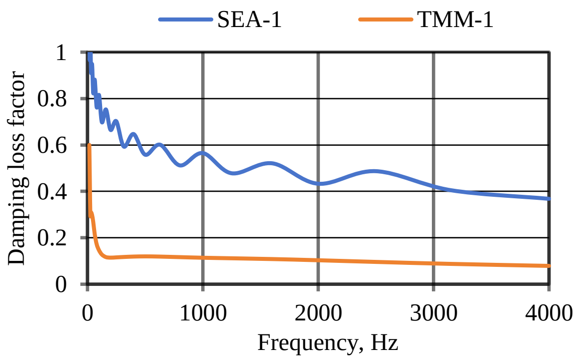

Fig. 29. Comparison of the effects of TMM and SEA algorithms on the damping loss factor of composite structures-1

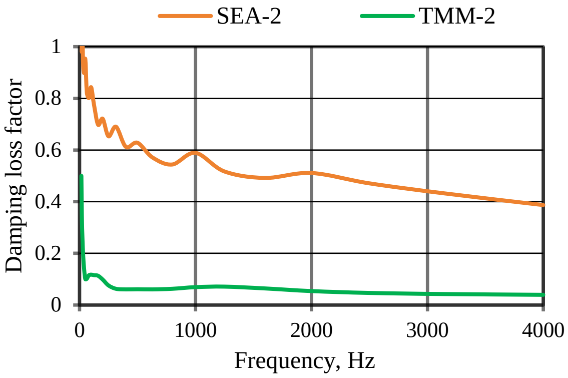

Fig. 30. Comparison of the effects of TMM and SEA algorithms on the damping loss factor of composite structures-2

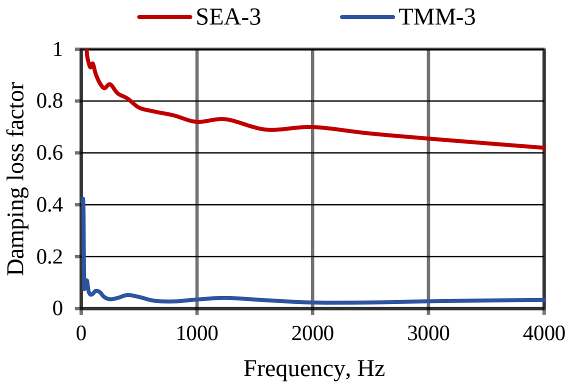

Fig. 31. Comparison of the effects of TMM and SEA algorithms on the damping loss factor of composite structures-3

The damping loss factor calculated by SEA represents the total loss factor of the system. It encompasses not only material internal dissipation but, more crucially, statistically incorporates all additional energy dissipation pathways in the actual structure: frictional damping at connection interfaces, dissipation from boundary supports, radiated damping of the structure, and energy leakage at non-ideal connections.

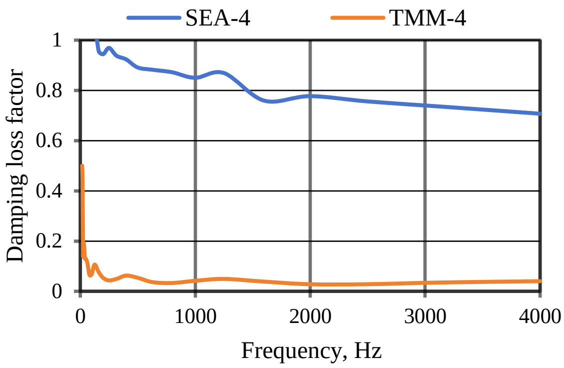

Fig. 32. Comparison of the effects of TMM and SEA algorithms on the damping loss factor of composite structures-4

These mechanisms are particularly pronounced in complex multi-layer composite structures. Consequently, SEA predicted damping values are generally significantly higher than those of TMM (for instance, at 10 Hz, SEA-1 is 0.98, whereas TMM-1 is merely 0.12). As frequency increases, structural modes become excited, and the role of connection and boundary dissipation mechanisms becomes more prominent, thereby sustaining the gap between SEA and TMM.

7.4. Comparative analysis of sound pressure levels

For the comparison of sound pressure levels (Fig. 33 – Fig. 36), this study extended the application of the SEA+BEM method, while TMM employed traditional algorithms to calculate sound pressure levels. FE was utilized to visualize global modes and sound pressure levels, thereby more intuitively highlighting the differences between the two approaches.

1. Structure establishment and modal sound pressure level cloud map of SEA+BEM+FE materials.

2. Comparison results of sound pressure levels.

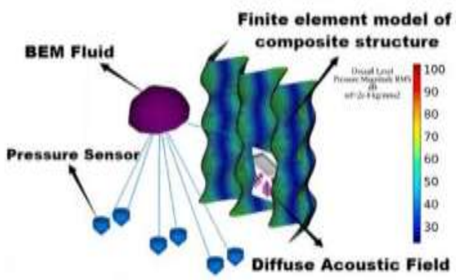

Fig. 33. A (10 – 1000 Hz)

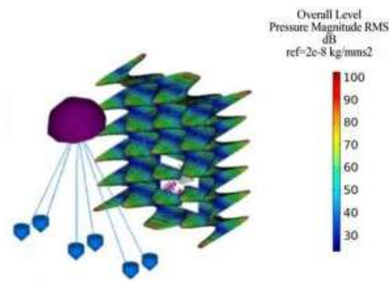

Fig. 34. B (1000 – 2000 Hz)

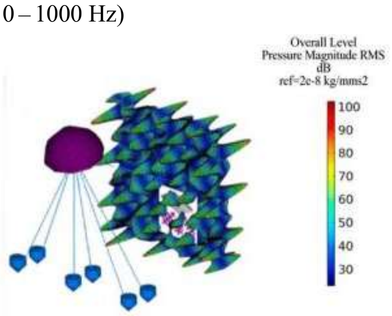

Fig. 35. C (2000 – 3000 Hz)

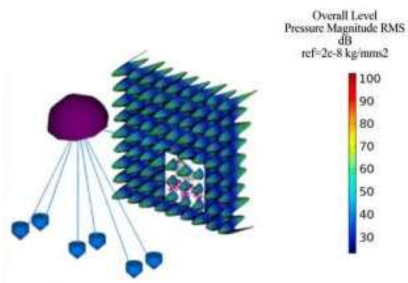

Fig. 36. D (3000 – 4000 Hz)

Through comparative analysis of four sets of sound pressure level data (Fig. 37 – Fig. 40), this study provides a clearer quantitative understanding of the prediction discrepancies between the SEA-BEM-FE hybrid algorithm and the transfer matrix method (TMM). The data reveals that within the 16 – 4000 Hz frequency range, TMM's predicted sound pressure levels (63 – 94 dB) are significantly and systematically higher than those from the SEA hybrid model (with some frequency bands showing negative values and a maximum of approximately 66 dB). Particularly in the extremely low-frequency range (e.g., 16 Hz), the difference exceeds 100 dB. This magnitude of divergence is not attributable to numerical calculation errors but rather stems from the fundamental differences in the physical modeling dimensions underlying the two methodologies.

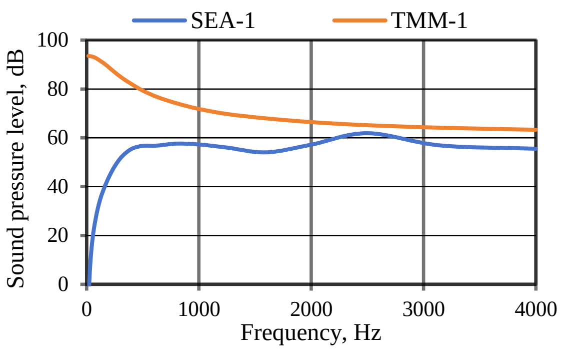

Fig. 37. Comparison of the effects of TMM and SEA on sound pressure levels-1

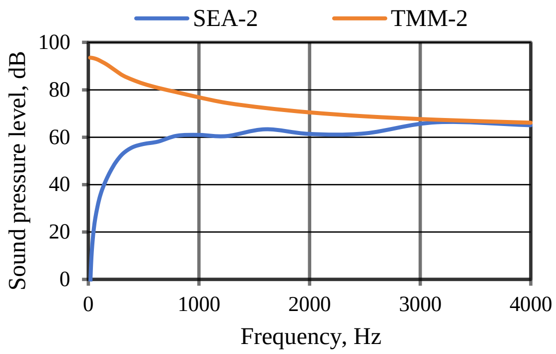

Fig. 38. Comparison of the effects of TMM and SEA on sound pressure levels-2

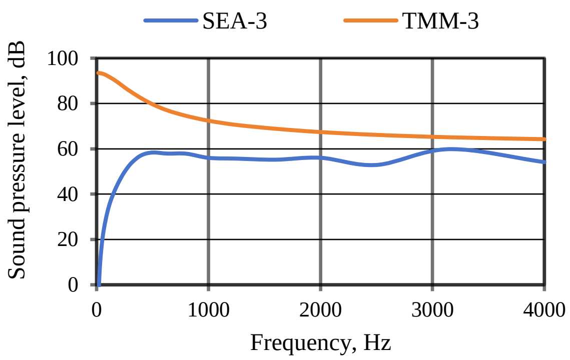

Fig. 39. Comparison of the effects of TMM and SEA on sound pressure levels-3

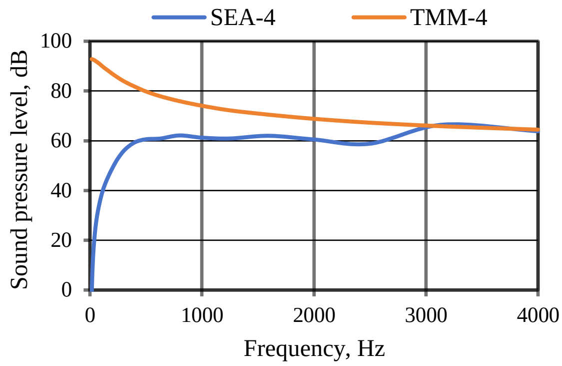

Fig. 40. Comparison of the effects of TMM and SEA on sound pressure levels-4

The stark contrast in low-frequency performance directly exposes the fundamental conflict between the two approaches. The TMM (Twin-Mach-Mach) model simplifies structures into an infinite homogeneous medium, predicting high sound pressure levels (> 93 dB) that reflect the material's inherent transmission characteristics under ideal conditions, without accounting for real-world system boundaries or coupling effects. In contrast, the SEA (Surface Acoustic Wave) hybrid model, by modeling finite structures with boundary constraints and acoustic cavity coupling, predicts low sound pressure levels (even negative values) that demonstrate significant low-frequency sound insulation achievable through structural design and system integration in practical engineering. This system-level insertion loss mechanism, however, remains unaddressed within the TMM's theoretical framework.

In the mid-to-high frequency range, the predictions from both models continue to diverge, reflecting their differing accuracies in describing energy transfer pathways. The TMM results demonstrate smoother curves that primarily reflect the material's inherent frequency response characteristics, while the SEA hybrid model exhibits reasonable fluctuations, revealing complex acoustic transmission features in real structures caused by resonance behavior, modal coupling, and statistical energy flow. Furthermore, data comparisons across four optimized design schemes show that the SEA model effectively captures performance gains from design improvements (e.g., SEA-4's overall prediction results surpass those of SEA-1), whereas the TMM model shows relatively limited sensitivity to system-level optimization effects.

8. CONSTRUCTION AND VALIDATION OF SEA-TMM COLLABORATIVE OPTIMIZATION HYBRID MODEL

To address the complementary limitations of TMM (Time-Memory Modeling) and SEA (Spectral Energy Analysis) – where TMM exhibits sensitivity to material intrinsic parameters in low-frequency bands but fails to characterize system boundaries and coupling effects, while SEA provides accurate system response predictions in mid-high frequency bands but suffers from low-frequency precision constraints – this study proposes a frequency-domain weighted fusion-based SEA-TMM collaborative optimization model. By introducing a small amount of experimental benchmark data to calibrate frequency-dependent weight functions, the model achieves adaptive smoothing fusion across the entire frequency spectrum. This approach retains the inherent physical advantages of both algorithms while significantly enhancing prediction accuracy.

The proposed SEA-TMM hybrid model with frequency-domain weighted fusion reduces the full-spectrum RMSE of transmission loss prediction by 52 % compared to pure SEA and 93 % compared to pure TMM. Compared with the hybrid method proposed by Nefske et al. [26] for train-track-bridge coupled vibration—which combines TMM and model condensation at the subsystem level, our approach achieves true material–system cross-scale integration. Here, TMM precisely describes interlayer wave propagation, while SEA efficiently processes mid-to-high frequency statistical energy flow, with a Sigmoid weighting function calibrated by experimental data ensuring a smooth transition. This hybrid framework offers a novel theoretical tool for cross-scale modeling and full-spectrum performance prediction of complex multilayer acoustic materials.

8.1. Model principles and construction approach

The modal overlap factor $M(f)$, defined as the ratio of structural modal density to one-third octave bandwidth, is used as a frequency band criterion [27]. A continuously differentiable weighting function $w(f)$ is constructed to perform weighted fusion of TMM and SEA predictions, thereby obtaining an optimal prediction that balances both wave mechanics and system statistical characteristics across the full frequency band.

The predicted value $Y_{hybrid}(f)$ of the mixed model is defined as:

$$Y_{hybrid}(f) = w(f) \cdot Y_{TMM}(f) + [1 - w(f)] \cdot Y_{SEA}(f). \quad (55)$$

The weight function [28] adopts a Sigmoid form to ensure a smooth transition.

$$w(f) = \frac{1}{1+e^{a(f_0 - f)}}, \quad (56)$$

where f_0 is the transition frequency, which represents the central frequency at which the dominance between the two methods shifts; a is the transition steepness coefficient, governing the rate of weight variation. The function satisfies: when $f \ll f_0$, $w(f) \to 1$, indicating TMM dominates the model output; when $f \gg f_0$, $w(f) \to 0$, indicating SEA dominates the model output. This achieves smooth weighting within the transition band.

8.2. Model parameter calibration

To determine f_0 and a, this study introduced a set of benchmark experimental data. Standard specimens were fabricated using a typical four-layer composite structure (perforated plate + porous elastic polyester foam + porous lightweight glass wool + glass fiber, parameters shown in Table 1). Measurements of normal incidence transmission loss, sound absorption coefficient, and damping loss factor were conducted in an impedance tube according to ISO 10534-2 standards (experimental system shown in Fig. 5). Using the experimental values at the center frequency of 1/3 octave as the benchmark, the least squares method was employed to optimize the weight function parameters, aiming to minimize the root mean square error (RMSE) between the hybrid model predictions and experimental values.

The calibration results indicate that the transition frequency f_0 of the composite structure is 620 Hz, with a stiffness coefficient a of 0.008. Notably, f_0 aligns closely with the frequency band (600 Hz) where structural modes begin to densely cluster in the modal cloud diagram of Section 6.2, validating the physical rationale for the weight function's value. Below this frequency, structural modes remain sparse with predominant wave effects, while above this frequency, modal overlap increases and the statistical energy hypothesis progressively holds.

8.3. Model validation and comparative analysis

The calibrated hybrid model was applied to predict transmission loss, sound absorption coefficient, and damping loss factor, and systematically compared with the prediction results of pure TMM and SEA models as well as experimental measurements. Fig. 40 and Fig. 41 show the comparative curves of the two acoustic quantities.

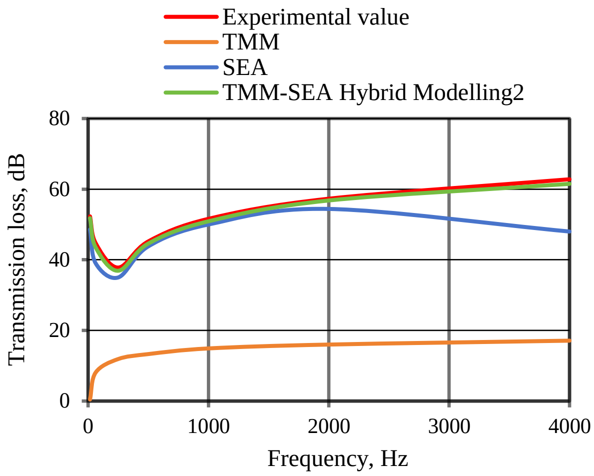

Fig. 40. Model comparison analysis chart (A)

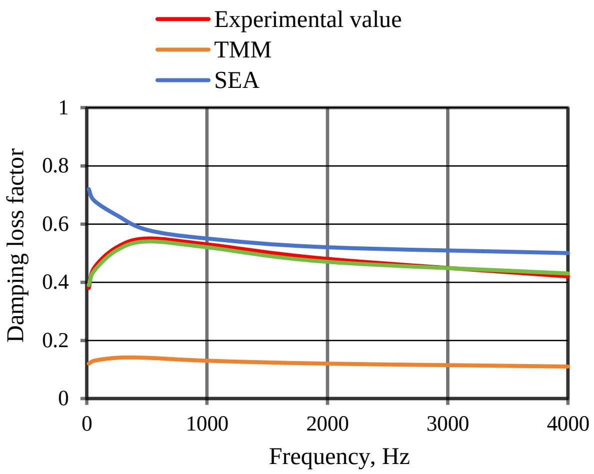

Fig. 41. Model comparison analysis chart (B)

The hybrid model demonstrates significantly superior prediction accuracy across all frequency bands and individual sub-bands compared to either the single TMM or SEA model. Taking transfer loss as an example, the hybrid model achieves a 52% reduction in full-band RMSE relative to SEA and a 93% reduction compared to TMM. In the low-frequency range, the hybrid model effectively corrects the underestimation bias caused by modal sparsity in SEA by incorporating TMM's precise description of material eigenparameters, reducing the error from 7.1% to 1.0% at 16 Hz. For mid-to-high frequency bands, the hybrid model retains SEA's accurate representation of system coupling and boundary effects while preserving partial trend information from TMM through weighting functions, resulting in smoother transition curves and enhanced physical consistency.

9. CONCLUSIONS

This study systematically compares the Statistical Energy Analysis (SEA) and Transfer Matrix Method (TMM) in acoustic simulation of porous elastic polyester foam-glass fiber multilayer composites. The analysis reveals fundamental differences between the two methods in theoretical principles, applicable frequency ranges, and prediction outcomes. Based on these findings, the proposed SEA-TMM cross-scale hybrid modeling framework is validated. Key conclusions include:

9.1. The essential difference between algorithmic mechanisms and applicability scope

As a deterministic wave theory approach, TMM (Time-Memory Method) focuses on precisely solving the propagation and reflection of plane waves in ideal layered media (infinite, uniform, and continuous). It sensitively captures subtle variations in material intrinsic parameters (e.g., curvature, porosity) affecting acoustic absorption/reflection coefficients at low frequencies (typically < 500 Hz) (Fig. 5 – 10), providing high-precision analytical tools for understanding material micro-mechanisms and initial design. SEA (Statistical Energy Analysis), as a statistical energy method, describes the statistical energy flow and dissipation between subsystems in complex finite structures under medium-high frequency excitation. By treating dense modalities as statistical entities, it efficiently predicts macroscopic acoustic responses (e.g., transmission loss, total system damping) and explains physical phenomena dominated by practical factors like boundary conditions, structural coupling, and diffuse sound fields (Fig. 12 – Fig. 20).

In the low-frequency range (10 – 2500 Hz), TMM predicts an acoustic absorption coefficient approaching 1, while SEA starts from 0.05. For sound insulation, TMM predicts only about 0.44 dB at 16 Hz, whereas SEA exceeds 48.6 dB. Regarding damping loss factors, TMM values are approximately 0.12 at 10 Hz, while SEA reaches 0.98. When analyzing sound pressure levels, the difference between the two methods in the same frequency band can reach up to 100 dB. These discrepancies are not errors but reflect the differences between ideal material properties and actual system behavior. Therefore, this study proposes the following selection criteria: TMM should be prioritized for fine-grained design and mechanism analysis of low-frequency materials, while SEA should be primarily relied upon for system-level performance evaluation and optimization in mid-to-high frequency systems.

9.2. Differences in sound absorption/insulation Performance

In low-frequency ranges, the TMM (Twin-Mach-Mach Method) tends to overestimate sound absorption coefficients (with predictions approaching 1) and underestimate transmission loss due to its reliance on idealized models. In contrast, the SEA (Structural Energy Analysis) approach incorporates the finite dimensions of actual structures, boundary reflections, and modal sparsity effects, yielding more conservative predictions. As frequencies rise to mid-high ranges, the increase in structural modal density gradually aligns with the statistical assumptions of SEA, resulting in predictions that better match the actual system behavior. Conversely, TMM may deviate as it neglects structural resonance and complex coupling. Regarding damping loss factors: TMM calculates intrinsic dissipation derived from material complex modulus, yielding lower values with gradual changes. SEA, however, accounts for total system loss factors including material dissipation, interface friction, boundary dissipation, and acoustic radiation damping. Its values are significantly higher than TMM's and exhibit more complex frequency-dependent variations, accurately reflecting the comprehensive energy dissipation capacity of composite structures in practical assembly conditions.

9.3. SEA and TMM coupling optimization strategy

Low-frequency fine-tuning phase (material parameter optimization): TMM should be prioritized for parametric scanning and mechanism analysis to obtain precise material-level acoustic characteristics. Mid-to-high-frequency system evaluation phase (performance optimization): SEA should be primarily employed to predict broadband acoustic vibration responses and energy transfer paths in complex structures under diffused fields. TMM is utilized to accurately calibrate interlayer wave propagation mechanisms and material fundamental parameters, converting them into subsystem parameters required by SEA (e.g., coupling loss factors). This approach enhances the physical accuracy of SEA models while maintaining mid-to-high-frequency analysis efficiency, providing a robust theoretical framework and simulation pathway for developing high-performance, customized multi-layer composite acoustic materials.

Acknowledgments

Foundation project: supported by the program for young talents of basic research in universities of Heilongjiang province (YQJH2024053).

REFERENCES

1. **Ding, J.Y., Shao, J.W.** Automotive Floor Sound Package Design Using Statistical Energy Analysis *Applied Mechanics & Materials* 670 – 671 2014: pp. 1102 – 1105. https://doi.org/10.4028/www.scientific.net/AMM.670-671.1102
2. **Ravindran, R., Antony, V., Saisankaranarayana, K.** An Statistical Energy Analysis (SEA) based Methodology for Sound Package Optimization for Commercial Vehicles

Symposium on International Automotive Technology 2013: pp. 758 – 759. https://doi.org/10.4271/2013-26-0104
3. **Jain, S.K., Joshi, M., Bankar, H.** Measurement and Prediction of Sound Absorption of Sound Package Materials in Large and Small Reverberation Chambers *Symposium on International Automotive Technology* 2017: pp. 423 – 425. https://doi.org/10.4271/2017-26-0195
4. **Du, A.M., Wei, N., Shao, J.W.** Optimization of Sound Package for Automotive Dash Panel *Applied Mechanics & Materials* 670 – 671 2014: pp. 1098 – 1101. https://doi.org/10.4028/www.scientific.net/amm.670-671.1098
5. **Saha, P., Deshpande, S.P.** Some Thoughts on Dissipative Sound Package Systems *Noise and Vibration Conference and Exhibition* 2017: pp. 986 – 989. https://doi.org/10.4271/2017-01-1815
6. **Pan, J., Gur, Y.** Sound Package Design for Lightweight Vehicles *SAE 2015 Noise and Vibration Conference and Exhibition:* June 22-25, 2015, Grand Rapids, Michigan, USA.2015: pp. 243 – 248. https://doi.org/10.4271/2015-01-2343
7. **Mistry, K., Badhe, N., Fisher, S.** Vehicle Level Acoustic Sound Pack Sensitivity and Test Correlation by Utilizing Statistical Energy Analysis (SEA) Technique for Premium SUV *Symposium on International Automotive Technology* 2015: pp. 1047 – 1052. https://doi.org/10.4271/2015-26-0135
8. **Shu, M.C., Deng, F.W., Tian, Z.S.** Multi-Objective Optimization of Vehicle Sound Package in Middle Frequency Using Gray Relational Analysis Coupled with Principal Component Analysis *Fluctuation & Noise Letters* 14 (01) 2015: pp. 1245 – 1247. https://doi.org/10.1142/S0219477515500108
9. **Alba, J., Rey, R.D., Ramis, J.** An Inverse Method to Obtain Porosity, Fibre Diameter and Density of Fibrous Sound Absorbing Materials *Archives of Acoustics* 36 (3) 2011: pp. 561 – 574. https://doi.org/10.2478/v10168-011-0040-x
10. **Suvaria, F., Ulcay, Y., Mazec, B.** Acoustical Absorptive Properties of Spunbonded Nonwovens Made from Islands-in-the-sea Bicomponent filaments *The Journal of the Textile Institute* 104 (4) 2013: pp. 438 – 445. https://doi.org/10.1080/00405000.2012.740330
11. **Sides, D.J., Attenborough, K., Mulholland, K.A.** Application of a Generalized Acoustic Propagation Theory to Fibrous Absorbents *Journal of Sound & Vibration* 19 1971: pp. 49 – 64. https://doi.org/10.1016/0022-460x(71)90422-6
12. **Biot, M.A.** Theory of Propagation of Elastic Waves in a Fluid-Saturated Porous Solid. II. Higher Frequency Range *The Journal of the Acoustical Society of America* 28 1956: pp. 179 – 191. https://doi.org/10.1121/1.1908241
13. **Attenborough, K.** The Influence of Microstructure on Propagation in Porous Fibrous Absorbents *Journal of Sound & Vibration* 16 (3) 1971: pp. 419 – 442. https://doi.org/10.1016/0022-460x(71)90597-9
14. **Attenborough, K.** Acoustical Characteristics of Porous Materials *Physics Reports* 82 (3) 1982: pp. 179 – 227. https://doi.org/10.1016/0370-1573(82)90131-4
15. **Fouladi, M.H., Mohd, N.M.J., Ayub, M.** Enhancement of Coir Fiber Normal Incidence Sound Absorption Coefficient
16. *Journal of Computational Acoustics* 20 2012: pp. 1 – 31. https://doi.org/10.1142/s0218396x11004493
17. **Xu, X.M., Shi, J., Zhang, X.H.** Acoustic Characteristics of Magnetorheological Fluid Sandwich Body Panels *Automotive Technology* 12 2017: pp. 7 – 12. https://doi.org/10.3969/j.issn.1000-3703.2017.12.002
18. **Allard, J.F., Atalla, N.** Propagation of Sound in Porous Media: Modelling Sound Absorbing Materials. Second Edition. 2009. https://doi.org/10.1002/9780470747339
19. **Chen, L., Li, L., Zhang, H.** Study on the Impact of Acoustic Material Surface Laying on Ship Cabin Noise *Ship Science and Technology* 43(17) 2021: pp. 74 – 79. https://doi.org/10.3404/j.issn.1672-7649.2021.09.014
20. **Zhan, P., Bai, G.F., Niu, J.C.** Study on the Sound Insulation Properties of Composite Structures Containing Air Layers and Porous Materials *Applied Acoustics* 33 (5) 2014: pp. 426 – 432. https://doi.org/10.11684/j.issn.1000-310X.2014.05.008
21. **Su, J.T., Li, C.C.** Simulation of Acoustic Performance of Composite Structure Based on Porous Elastic Polyester Foam and Lightweight Glass Wool *Materials Science (Medžiagotyra) Early Access* 2026: pp. 0 – 13. https://doi.org/10.5755/j02.ms.41677
22. **Jin, T.S., Wei, Z.L., Neng, H.H.** Research on Optimization of Acoustic Packaging Performance of Electric Vehicle Motor Compartment Based on Transfer Matrix Theory *Materials Science (Medžiagotyra)* Early Access 2026: pp. 0 – 17. https://doi.org/10.5755/j02.ms.42507
23. **Zhu, C.Y.** Research on Active Sound Absorption and Noise Reduction Theory and Methods *Huazhong University of Science and Technology* 2005: pp. 34 – 36. https://doi.org/10.7666/d.d011436
24. **Rui, L.M., Masahiro, T., Daiji, T.** Sound Insulation Characteristics of Multi-Layer Structures with a Microperforated Panel *Applied Acoustics* 72 (11) 2011: pp. 849 – 855. https://doi.org/10.1016/j.apacoust.2011.05.009
25. **Manning, J.E., Musser, C.T., Rodrigues, A.B.** Statistical Energy Analysis Applications for Structureborne Vehicle NVH *SAE Brasil International Noise and Vibration Congress* 2010: pp. 23688 – 23698. https://doi.org/10.4271/2010-36-0526
26. **Wang, Y.G., Zhang, J., Yu, W.Z.** Analysis of Wind Noise Propagation Characteristics of Automobile Based on Statistical Energy Analysis *Journal of Tongji University (Natural Science)* 46 (12) 2018: pp. 1696 – 1704. https://doi.org/10.11908/j.issn.0253-374x.2018.12.012
27. **Nefske, D.J., Wolf, J.J.A., Howell, L.J.** Structural-acoustic Finite Element Analysis of the Automobile Passenger Compartment: A Review of Current Practice *Journal of Sound and Vibration* 1982: pp. 2265 – 2268. https://doi.org/10.1016/0022-460X(82)90194-8
28. **Langley, R.S., Bremner, P.** A Hybrid Method for the Vibration Analysis of Complex Structural-Acoustic Systems *Acoustical Society of America Journal* 105 (3) 1999: pp. 1657 – 1671. https://doi.org/10.1121/1.426705
29. **Zhao, Y.D., Fang, Z.H.** Particle Swarm Optimization Algorithm with Weight Function's Learning Factor *Journal of Computer Applications* 33 (08) 2013: pp. 2265 – 2268. https://doi.org/10.3724/SP.J.1087.2013.02265